Check for updates

Buoy-based monitoring of sea surface carbon dioxide partial pressure at Qingdao coastal area

Lu Cao[1,2], Su Li[1], Shuwei Zhang[1,2], Ning Wu[1,2], Keke Zhang[1,2], Wenqing Li[1,2], Ran Ma[1,2], Dongzhi Chu[1,2], Ni Wang[1,3]* and Yan Liu[1,2]*

[1]Qilu University of Technology (Shandong Academy of Sciences), Institute of Oceanographic Instrumentation, Qingdao, China, [2]Ocean Observation and Exploration Research Department, Laoshan National Laboratory, Qingdao, China, [3]Faculty of Information Science and Engineering, Ocean University of China, Qingdao, China

Continuous time series observations of seawater carbon dioxide partial pressure (pCO$_2$) are crucial for documenting temporal variations in air-sea CO$_2$ fluxes. To examine the seawater pCO$_2$ variation and its influence factors at Qingdao coastal waters, a high-resolution observation of seawater pCO$_2$ near the Xiaomaidao Island was conducted from May 29 to July 25 in 2024. Sea surface pCO$_2$ varied from 519 µatm to 717 µatm during this monitoring period, with an obvious decline and rise from July 12 to 21. The variation of seawater pCO$_2$ was mainly affected by the increasing sea surface temperature, except for the period of pCO$_2$ decrease which was caused by *Ulva prolifera* bloom. Accompanied by the increase of *U. prolifera*, sea surface pCO$_2$ decreased to 563 µatm, then the coverage of *U. prolifera* decreased and sea surface pCO$_2$ rose to 669 µatm during period of July 12 to 21. The observation site acted as a source for atmospheric CO$_2$ throughout the monitoring period, with air-sea CO$_2$ flux ranging from less than 1 mmol m^{-2} d^{-1} to over 100 mmol m^{-2} d^{-1}, resulting in a total CO$_2$ release of 334 mmol m^{-2}. Thus, it is essential for high-resolution measurement of pCO$_2$ in coastal areas.

KEYWORDS

carbon dioxide partial pressure, Qingdao Coast, *Ulva prolifera* influence, early bloom, CO2 flux

1 Introduction

The ocean is the largest reservoir of carbon, absorbing approximately 30% of the anthropogenic CO$_2$ emitted into the atmosphere (Sabine et al., 2004). This process has induced ocean acidification and variations of carbonate system (Doney et al., 2009; Mostofa et al., 2016). Ongoing global warming and associated climate changes are expected to alter CO$_2$ fluxes at the air–sea interface and the regulatory mechanism. Therefore, regular assessment of the temporal and spatial variabilities of marine pCO$_2$ is urgently needed for research on carbon cycle and carbon budgets (Murata et al., 2022; Regnier et al., 2022; Wu et al., 2024).

The coastal region significantly influences the carbon cycle (Cai, 2011; Dai et al., 2022). Due to the strong terrestrial input and anthropogenic disruptions in coastal regions, the carbonate system and CO_2 flux exhibit complex fluctuations (Lin and Lin, 2022; Xue et al., 2016), leading to alteration of coastal waters function as source or sink to atmospheric CO_2. The temporal variations of seawater pCO_2 influenced by factors such as temperature effects, mixing processes, biological processes and air-sea exchange and other contributing processes (Borges et al., 2006; Xue et al., 2016). As a transition zone connecting the southern Yellow Sea with Jiaozhou Bay, the Qingdao coastal region is strongly affected by anthropogenic activities and green tides. The green tides caused by *U. prolifera* have occurred annually in the southern Yellow Sea since 2007, usually appearing along the Qingdao coast in June and dissipating in August or early September (Yuan et al., 2022; Shao et al., 2024; Zhang et al., 2019). The *U. prolifera* bloom has resulted in extensive harm to the ecology and economy of coastal cities and led to significant alterations in the carbon system (Zhang et al., 2019; Xiong et al., 2023). Thus, the time series observation is essential for further understanding the temporal variation in seawater pCO_2 and its associated influencing factor. In particular, the impact of *U. prolifera* on the carbonate system in Qingdao coast was mainly studied previously based on cruises sample collection (Hu et al., 2024; Li et al., 2021; Xiong et al., 2023; Deng et al., 2018; Hu et al., 2015), and lack of continuous high-resolution observations.

In this work, a time serious observation based on buoy near the Xiaomaidao Island at Qingdao coastal area was conducted during May 29 – July 25, 2024. Based on the collected data, we reported the variation in seawater pCO_2 and the air–sea CO_2 flux, identified the factors affecting the temporal changes in seawater pCO_2, and explored the continuous influence of *U. prolifera* bloom on seawater pCO_2.

2 Materials and methods

2.1 Study site

The observation site (120.44°E, 36.05°N) is located at Qingdao coastal area (Figure 1), near Xiaomaidao Island, and is in a transition zone connecting the southern Yellow Sea with Jiaozho Bay. This site is dominated by semi-diurnal currents, with a water depth of about 23 m. The rainfall is highest in summer and lowest in winter, with an average annual precipitation of approximately 660 mm (http://www.qingdao.gov.cn). The investigation area is affected by the southeast monsoon and coastal waters in summer. The sea surface salinity (SSS) is the highest in winter, and the peak sea surface temperature (SST) generally occurs in August. Since 2007, *U. prolifera* has occurred annually in the southern Yellow Sea, and Qingdao is one of the cities receiving the macroalga.

2.2 Field observations based on buoy

The 15 m intelligent buoy was deployed at the observation site from May 29 to July 25 in 2024. There was an air-water equilibrator (MAPCO$_2$) (Friederich et al., 1995; Sutton et al., 2014) placed in the buoy shaft floating on the sea surface based on float, and a customized gas control module and standard gas (Figure 2) fixed in the buoy chamber without contact with seawater for pCO_2 measurement. During monitoring, the seawater pCO_2 was measured with a frequency of 1 h or 2 h and the calibration frequency was 24 h. The atmosphere pCO_2 data which was measured at sit on May 29, 2024, was used for air-sea CO_2 flux calculation. The sea surface temperature (SST) and sea surface salinity (SSS) were determined by SBE37 (Sea-bird Scientific). The dissolved oxygen saturation (DO%) which refers to the ratio of seawater DO content to its solubility, was measured using the probe developed by the institute of Oceanographic Instrumentation. The wind speed was measured using an ultrasonic anemometer (windmaster pro, Gill Instruments) installed at a height of 10 m.

2.3 Determination of pCO_2

The *in-situ* non-dispersive infrared (NDIR) seawater pCO_2 instruments (Fietzek et al., 2014; Sutton et al., 2014; Hunt et al.,
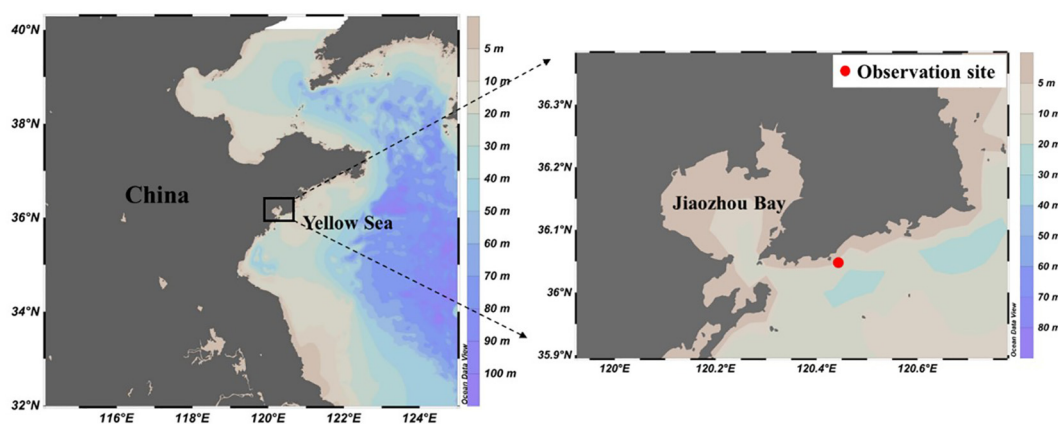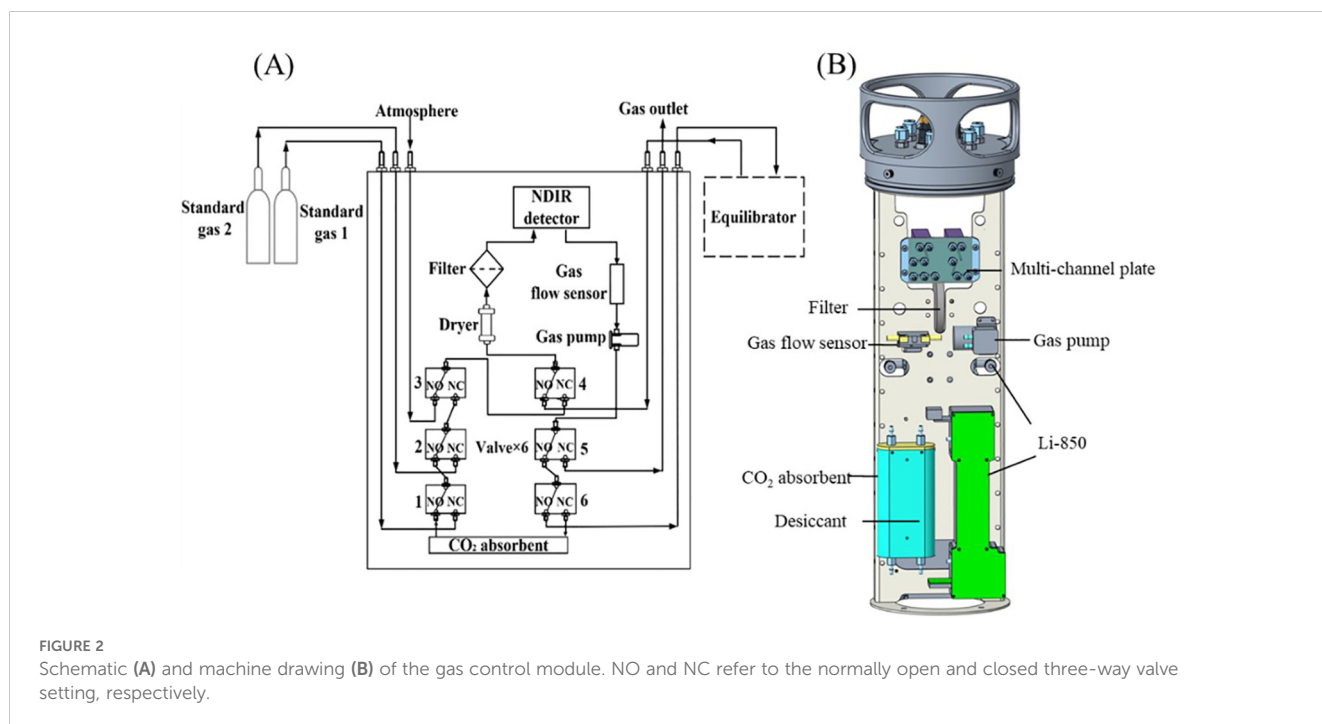

FIGURE 1
Location of observation site near the Xiaomaidao Island.

FIGURE 2
Schematic **(A)** and machine drawing **(B)** of the gas control module. NO and NC refer to the normally open and closed three-way valve setting, respectively.

2017; Ribas-Ribas et al., 2018) are often employed on the buoy to describe the temporal variations of $p\text{CO}_2$ and CO_2 fluxes at the air-sea interface (Atamanchuk et al., 2015; Xue et al., 2016; Liu Q. et al., 2019). They used the gas-permeable membrane (Fietzek et al., 2014) or continuous bubbling air–water equilibrator (Sutton et al., 2014) to equilibrate the headspace air with seawater. After equilibration, the CO_2 composition of headspace air reflects that of seawater. The evaluation and comparison of commercial *in-situ* $p\text{CO}_2$ instruments demonstrated that the system employing bubble equilibration technique (Sutton et al., 2014) had high accuracy and stability (Alliance for Coastal Technologies, 2010a, b, c). Though the commercial *in-situ* instrument using bubble equilibration (MAPCO$_2$) is widely used, it is sometimes inflexible for installation, inconvenient self-maintenance and expensive. The water quality monitoring buoys have been well developed by integrating biochemical sensors, optical devices for absorption, fluorescence and scattering, and communication devices (Błażejewski et al., 2024, 2023; Agade et al., 2022; Ng et al., 2012) for field applications. Therefore, easily integrated seawater $p\text{CO}_2$ instruments are needed for future collaborative observations.

To flexible investigate the seawater $p\text{CO}_2$ variations in Qingdao coastal waters, a customized and concise gas control module combined with standard gas (National Standard Material Research Center) and the bubble equilibrator of MAPCO$_2$ (Friederich et al., 1995; Sutton et al., 2014) which connects gas control module with two gas pipelines were deployed on a 15m intelligent buoy in this article. The module operates in three modes: seawater measurement, atmosphere measurement and calibration modes (Figure 2A). During seawater $p\text{CO}_2$ measurement, the gas driven by pump circularly goes out from the gas pipe (1.6 mm i.d., 3.2 mm o.d.) beneath seawater surface and continuously bubbles in the equilibrator which floated on the sea surface, then the gas returns to the gas control module through the other pipe (3.2 mm

i.d., 6.4 mm o.d.). The equilibrator was made of copper-nickel alloy to prevent biofouling. More details for bubble equilibrator can be found in the paper by Sutton et al. (2014). During monitoring, the control module timed measured standard gas by switching different modes. The 12V voltage for gas control module was provided by buoy's solar power, and data is transmitted over 3G/4G networks.

The gas control module is housed in a sealed cylindrical cabin, including NDIR detector (Licor850, LI-COR Biotechnology), gas flow sensor (AWM3300, Honeywell Automation & Control, Inc.), desiccant (silica gel), CO_2 absorbent (soda lime), filter (1.0 μm), gas pump (KLVP-SB12, Kamoer Fluid Tech Shanghai Co., Ltd., China), electromagnetic three-way valves (LVM105R-6B, SMC), customized multi-channel plate, gas pipe and the control circuit (Figure 2). The NDIR detector measures mole fraction of CO_2 ($x\text{CO}_2$) and H_2O ($x\text{H}_2\text{O}$) in gas path at about 51.5 °C, and has a thermal insulation cavity outside to ensure the stability and accuracy measurements. The desiccant is used to absorb vapor in the gas path. The soda lime is used to absorb CO_2 during zero gas calibration. The gas flow sensor is used to monitor the condition of system during measurement. The three-way valves were connected to the gas pipe through channels (diameter 1.5 mm) inside the multi-channel plate (Figure 2B). The gas control module could be operated in different modes based on the positions of three-way valves, similar to other instruments. The gas control module has the characteristics of simple structure and good integration.

Given the lack of drying methods for long-term autonomous measurements, the determined $x\text{CO}_2$ should be converted to dry $x\text{CO}_2$. Finally, the $p\text{CO}_2$ of seawater at 100% humidity was calculated.

The dry $x\text{CO}_2$ was calculated using the following equation:

$$x\text{CO}_2^{dry} = \frac{x\text{CO}_2}{1 - x\text{H}_2\text{O}} \tag{1}$$

where the xCO_2^{dry} (μmol mol^{-1}) is xCO_2 in dry air, and xCO_2 (μmol mol^{-1}) and xH_2O (mol mol^{-1}) denote the measured concentrations.

The partial pressure of the surface seawater CO_2 (pCO_2, μatm) is calculated as follows:

$$pCO_2 = xCO_{2\,corr}^{dry} \times (p - VP^{H_2O}) \qquad (2)$$

$$VP^{H_2O} = \exp\left(24.4543 - 67.4509 \times \left(\frac{100}{t + 273.15}\right)\right.$$
$$\left. - 4.8489LN\left(\frac{t + 273.15}{100}\right) - 0.000544 \times S\right) \qquad (3)$$

where $xCO_{2\,corr}^{dry}$ is the corrected xCO_2, p denotes the pressure (atm) of atmosphere, and VP^{H_2O} refers to the water vapor pressure at 100% humidity obtained using the *in-situ* temperature (t, °C) and salinity (S) (Weiss and Price, 1980).

The precision of the pCO_2 measurement system was evaluated through repeated measurements of seawater samples, and the results were expressed as standard deviation (SD) of xCO_2. The seawater samples were adjusted to various pCO_2 values using NaOH and HCl solutions. Table 1 shows the precision of the seawater pCO_2 measurement system during repeated measurements of three seawater samples in the laboratory. With xCO_2 values in the range of 390–800 μmol mol^{-1}, the measurement system exhibited a precision better than 1 μmol mol^{-1}, with the SD ranging from 0.67 μmol mol^{-1} to 0.84 μmol mol^{-1}. Good precision here provides a prerequisite for obtaining good accuracy.

The accuracy was evaluated by comparing with an underway seawater pCO_2 instrument (GO8050, General Oceanics, INC.). The accuracy was expressed as the relative error of xCO_2 (Table 2). Prior to comparison, the underway instrument was calibrated using standard gases. For comparison, equilibrator and water pump of the underway instrument were placed in a thermostatic bath containing the seawater samples. The accuracy was estimated in a xCO_2 range of 200 – 1000 μmol mol^{-1} through adjustment of seawater with HCl and NaOH solutions. The average of 10 continuous measurements obtained by the GO8050 analyzer after equilibrium was considered the true value. In the xCO_2 range of 200 – 1000 μmol/mol, the error was -5.1 – 2.3 μmol mol^{-1}, and the relative error was within 1%.

2.4 Data processing

To eliminate the thermodynamic influence of temperature, we normalized pCO_2 to the average temperature of the investigation

TABLE 1 Precision test in the laboratory.

xCO_2 (μmol mol^{-1})	Standard Deviation (μmol mol^{-1})	Measurements
390.0	0.79	10
633.8	0.67	6
799.5	0.84	8

TABLE 2 Accuracy test in the laboratory.

Measured xCO_2 of developed instrument (μmol mol^{-1})	Measured xCO_2 of GO (μmol mol^{-1})	Error (μmol mol^{-1})	Relative error
226.7	229.0	-2.3	1.0%
467.0	467.6	-0.6	0.1%
605.1	602.8	2.3	0.4%
1065.7	1070.8	-5.1	0.5%

($npCO_2$) by Takahashi et al. (1993):

$$npCO_2 = pCO_2 \times \exp(0.0423 \times (t_m - SST)) \qquad (4)$$

where $npCO_2$ is the normalized pCO_2, and t_m denotes the average temperature during the time series monitoring. Meanwhile, simulated pCO_2 changes solely caused by temperature could be calculated when SST is the initial temperature and t_m is the observed temperature.

Air–sea CO_2 flux (FCO_2, mmol m^{-2}d^{-1}) was estimated according to the following equation:

$$FCO_2 = k \times K_0 \times (pCO_{2\,water} - pCO_{2\,air}) \qquad (5)$$

where k indicates the gas transfer velocity, K_0 represents the solubility coefficient of CO_2 (Weiss, 1974), and pCO_{2water} and pCO_{2air} are the pCO_2 in the surface water and atmosphere, respectively. k was estimated using the formula proposed by Sweeney et al. (2007).

$$k = 0.27 \times U_{10}^2 \times (Sc/660)^{-0.5} \qquad (6)$$

where U_{10} (m s^{-1}) refers to the wind speed at 10 m height. Sc denotes the Schmidt number of CO_2 in seawater (Wanninkhof, 1992). In this paper, a positive value of FCO_2 denoted CO_2 release from water to the atmosphere.

3 Results and discussion

3.1 Variations of monitoring data at coastal site

During the buoy-based time series observation period of May 29 – July 25, 2024, *U. prolifera* bloom was observed at Qingdao coastal region based on satellite remote images. Its coverage increased in mid-July and then decreased in late July (Figure 3). The SST increased from approximately 16°C to 22°C (Figure 4A) due to the increase in solar radiation. By contrast, SSS showed a decreased trend and ranged from ~31.0 PSU to ~29.2 PSU (Figure 4A). The sudden decrease in SSS during the observation period was possibly due to rainfall. On the days when the salinity dropped to about 29.2 PSU (July 8, July 16 and July 22), the daily rainfall at the observatory near Xiaomaidao Island was 58 mm, 39 mm and 48 mm, respectively (http://swglj.qingdao.gov.cn). During the observation period, the tidal height varied between 56 cm and 437 cm (Figure 4B). DO% also showed a general downward trend,
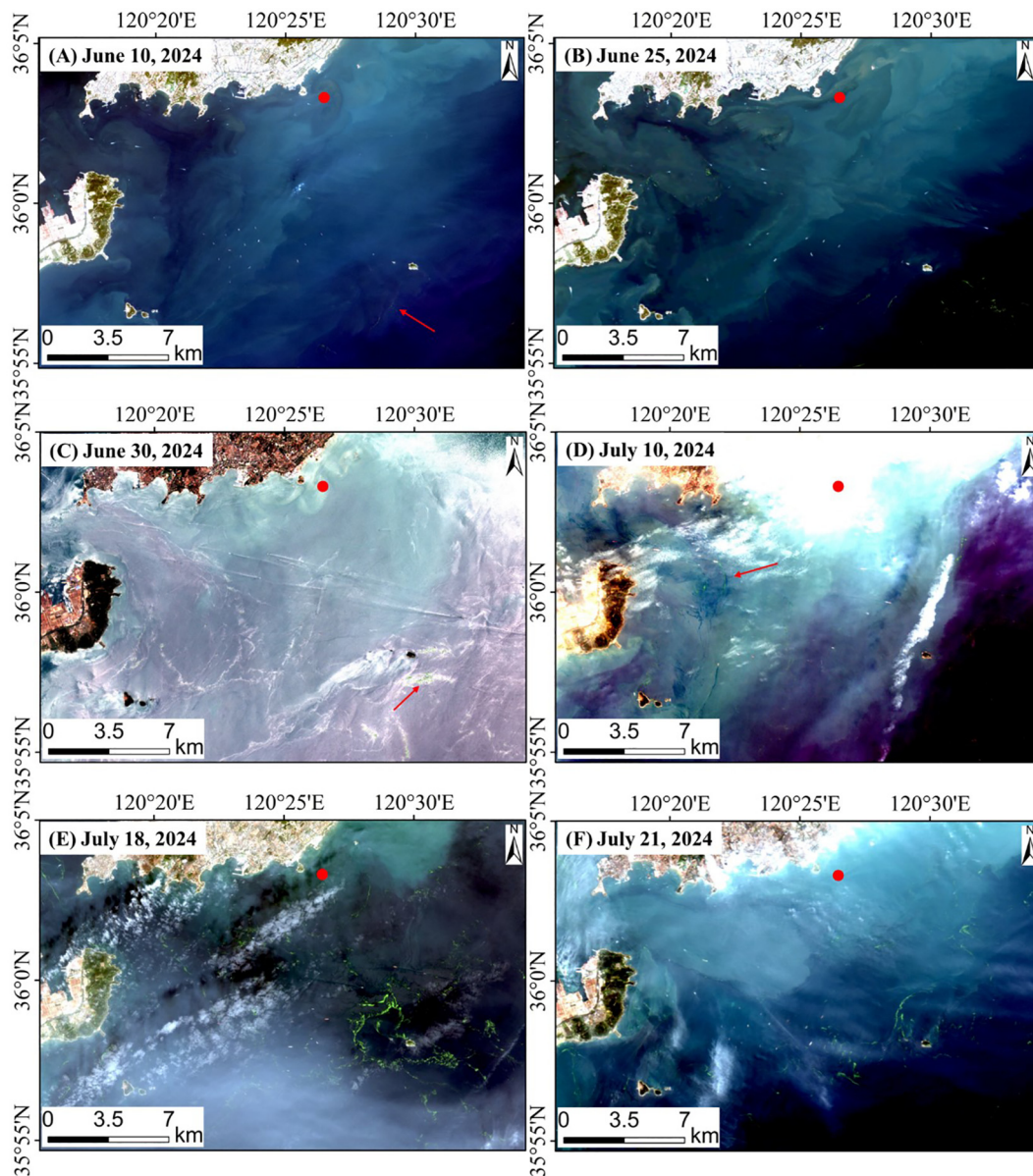
FIGURE 3
Satellite images of *U. prolifera* distribution. Panels **(A-F)** showed the distributions of *U. prolifera* on June 10, June 25, June 30, July 10, July 18 and July 21, 2024, respectively. These images were obtained using the monitoring data of GF-6 WFV and HJ-2A/2B CCD satellites (https://www.cresda.com/zgzywxyyzx/index.html) with 16m spatial resolution. The *U. prolifera* on June 10, June 30 and July 10 were indicated by red arrows.

varying within a range of 112% to 89% during the investigation period, and temporarily high values were observed in July (Figure 4D). Sea surface pCO_2 ranged from 519 µatm to 717 µatm, with an average of 615 ± 45 µatm, and the daily average sea surface pCO_2 increased by ~110 µatm at the end of observation compared with that in the beginning (Figure 4C). While the $npCO_2$ of seawater showed a slightly decreasing trend, and a ~30 µatm lower daily average $npCO_2$ was observed at the end of observation compared with that in the beginning (Figure 4D). In addition, both surface pCO_2 and $npCO_2$ showed a rapid decline and rise from July 12 to 21, and then the values remained stable.

The atmospheric pCO_2 was 417 µatm, which is lower than that of seawater. Thus, this observation site served as a CO_2 source for the

atmosphere throughout the observation period in 2024. The wind speed ranged from 0.1 m s^{-1} to 18.5 m s^{-1}, and the average was 3.0 m s^{-1} (Figure 4E). The large variations in wind speed and seawater pCO_2 induced considerable changes in CO_2 flux. The influence of wind speed is particularly important. According to Equation 6, the influence of wind speed on CO_2 flux is quadratic. The CO_2 flux ranged from less than 1 mmol m^{-2} d^{-1} to over 100 mmol m^{-2} d^{-1}, roughly consistent with wind speed, with an average value of 5.9 mmol m^{-2} d^{-1} (Figure 4F). Furthermore, the variations in CO_2 flux during the observation period demonstrated the importance of high-resolution monitoring in carbon flux estimation. Based on collected data, the seawater at investigation site near Xiaomaidao Island released 334 mmol CO_2 m^{-2} to the atmosphere during May 29 – July 25, 2024.
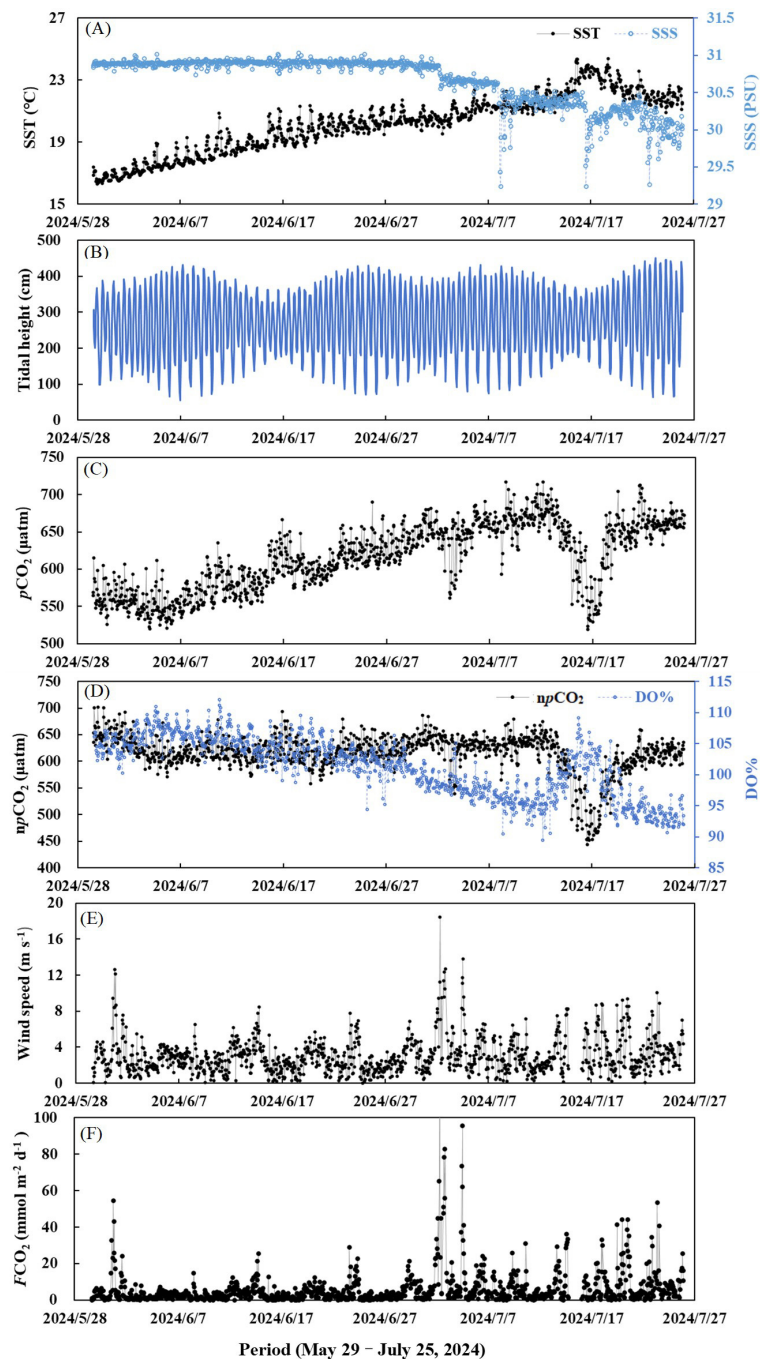
FIGURE 4
Variations in SST and SSS **(A)**, tidal height **(B)**, surface pCO_2 **(C)**, $npCO_2$ and DO% **(D)**, wind speed **(E)**, and FCO_2 **(F)** from May 29 to July 19, 2024.

The data collected in the western part of the southern Yellow Sea which lies approximately between 33°N and 37°N and west of the 50m isobath (Wang and Zhai, 2021) and Jiaozhou Bay (Li et al., 2023) during summer were compared with the investigation results of this study (Table 3). It was shown that the western part of the southern Yellow Sea had relatively lower SST, seawater pCO_2, CO_2 flux, and higher SSS, while lower SSS accompanied with higher SST, seawater pCO_2 and CO_2 flux were observed in Jiaozhou Bay compared with this study. During summer the Jiaozhou Bay

became a strong source of atmospheric CO_2. In addition to the higher SST, terrestrial inputs were also the reason for the high sea surface pCO_2 and CO_2 flux in Jiaozhou Bay. It was reported that except for the Dagu River, most rivers in Jiaozhou Bay had no pristine runoff and almost became channels of wastewater which was abundant in pCO_2, resulting in the high seawater pCO_2 values observed in Jiaozhou Bay (Gao et al., 2008; Li et al., 2023). Though there was no freshwater input from rivers near Xiaomaidao Island, the Qingdao coast area was significantly disturbed by human

TABLE 3 Means and ranges (in brackets) of SST, SSS, seawater pCO$_2$, and FCO$_2$ at the time series site during 2024 and comparisons of these data with those obtained on the western part of southern Yellow Sea and the Jiaozhou Bay from literature.

Time	SST (°C)	SSS	pCO$_2$ (μatm)	FCO$_2$ (mmol m^{-2} d^{-1})
Coastal time series site near Xiaomaidao Island (This study)				
2024 – 06 (1 – 30 Jun, 2019)	19.1 ± 1.2 (16.5 – 21.7)	30.9 ± 0.04 (30.7 – 31.0)	593± 35 (520 – 690)	3.4 ± 3.9
2024 – 07 (1 – 25 Jul, 2019)	21.8 ± 0.9 (19.5 – 24.4)	30.4 ± 0.3 (29.2 – 31.0)	648 ± 35 (519 – 717)	9.1 ± 14.4
Western part of southern Yellow Sea (Wang and Zhai, 2021)				
2011 – 06	17.8 ± 1.6 (15.0 – 20.4)	31.6 ± 0.3 (31.0 – 32.0)	430 ± 69 (323 – 538)	2.6 ± 4.3
2016 – 07	21.7 ± 1.7 (18.4 – 24.0)	30.9 ± 1.1 (28.4 – 31.9)	440 ± 130 (221 – 574)	3.6 ± 9.2
Jiaozhou Bay (Li et al., 2023)				
13 Jun. 2014	21.39 ± 1.54	30.52 ± 0.34	675 ± 138	17.4 ± 6.9
01 Jul. 2014	23.14 ± 1.22	30.63 ± 0.15	723 ± 118	17.6 ± 5.1

activities (Yang et al., 2018; Liu X. et al., 2019), making its sea surface pCO$_2$ higher than that of the western part of the southern Yellow Sea.

3.2 Factors affecting sea surface pCO$_2$ during time serious observation

The temporal variation of seawater pCO$_2$ in coastal regions resulted from the interaction of multiple processes, at least including temperature effect, air-sea CO$_2$ exchange, mixing processes and phytoplankton activity (Borges et al., 2006; Xue et al., 2016). Consistent with other studies of seawater pCO$_2$ (Xue et al., 2016; Hu et al., 2024; Li et al., 2023), we used Pearson correlation analysis to explore the factors affecting sea surface pCO$_2$ variations, where the square of the correlation coefficient r^2 represents relevance and the p-value of less than 0.01 in the analysis results represented 99% confidence level (Figure 5). Consistent with the ~6 °C increase in SST, sea surface pCO$_2$ except for the low values from July 12 – 21 showed an increasing trend during the time series monitoring, and it was strongly positive correlated with SST (r^2 = 0.76, p<0.01) (Figure 5A), indicating the important influence of increasing temperature on the variations in pCO$_2$ during this period. In addition, the temperature driven pCO$_2$ values simulated according to the model proposed by Takahashi et al. (1993) were in good agreement with the observed values except for the low values during July 12 – 21 (Figure 5A), also suggesting the major control of SST on seawater pCO$_2$ during this period. However, the daily average temperature simulated pCO$_2$ value on July 25 was 34 μatm higher than that of the observed value, indicating influence of other factors.

By normalizing the pCO$_2$ values to the average SST, npCO$_2$ values were obtained to evaluate influence of other factors on sea surface pCO$_2$. SSS showed a decreased trend in this study, while npCO$_2$ did not evidently increase, and no correlation between npCO$_2$

and tide (Figure 5B), suggesting that the influence of terrestrial inputs with abundant pCO$_2$ was offset by other processes, such as biological activity and air-sea CO$_2$ exchange. During the whole observation period, the decreased trend of DO% and a ~30 μatm decrease in npCO$_2$ implied that biological activity was not an important factor controlling the seawater pCO$_2$ change. Considering the slight decrease in the level of npCO$_2$ during the overall period, the release of CO$_2$ from seawater to atmosphere in the air–sea exchange process may also influence the pCO$_2$ variations.

3.3 *U. Prolifera* blooms affecting sea surface pCO$_2$

Since July 12, both the surface pCO$_2$ and npCO$_2$ showed an obvious decrease and the daily average of seawater pCO$_2$ and npCO$_2$ reached the lowest on July 16 – 17, with values of 563 μatm and ~488 μatm, respectively, which were 116 μatm of pCO$_2$ and 147 μatm of npCO$_2$ lower than those in July 12, and then the daily average pCO$_2$ and npCO$_2$ value increased to 669 μatm and 615 μatm on July 21, respectively. On the contrary, the daily average DO % reached ~102% on July 16 – 17 and then decreased. The npCO$_2$ exhibited a negative correlation with DO% during July 12 – 21 (r^2 = 0.51, p<0.01) (Figure 5C), indicating the important influence of biological activity on the variation in pCO$_2$ during this special period.

Based on satellite remote images, *U. prolifera* was observed to increase obviously on July 18 (Figure 3E), which was roughly consistent with the date of the seawater pCO$_2$ reduction, indicating the influence of *U. prolifera* bloom on carbonate system. The rapidly decreasing pCO$_2$ and increasing DO% in seawater was caused by the biological production of *U. prolifera*. It was reported that at the early bloom stage, photosynthesis of macroalga can quickly absorb dissolved inorganic carbon in seawater, leading to a decrease of pCO$_2$ in seawater (Li et al.,
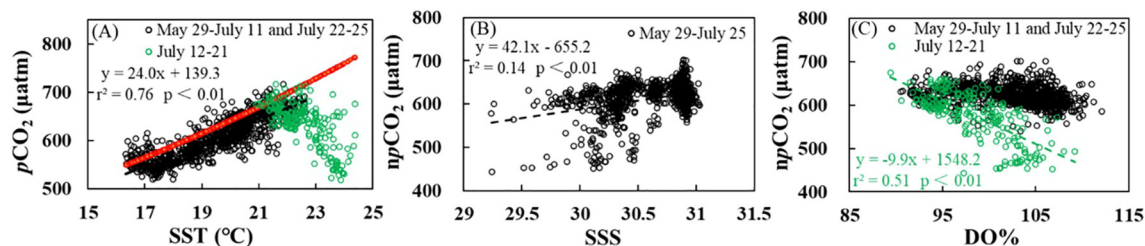
FIGURE 5
Sea surface pCO_2 versus SST **(A)**, $npCO_2$ versus SSS **(B)**, and $npCO_2$ versus DO% **(C)** from May 29 to July 25, 2024. Positive correlation between pCO_2 and SST on May 29 – July 11 and July 22 – 25, and negative correlation between $npCO_2$ and DO% on July 12 – 21 were observed. In panel **(A)**, red lines indicate simulated pCO_2 driven by temperature variations based on Equation 4.

2014; Zhang et al., 2019). The cruise investigation at offshore area of Qingdao (Hu et al., 2024) also showed the decreased dissolved inorganic carbon and increased pH in seawater during bloom phase. Subsequently, as shown in satellite image on July 21 (Figure 3F), the amount of *U. prolifera* decreased, which may be caused by manual cleaning and sink of the decaying macroalga. Thus, the rising pCO_2 and decreased DO% in seawater after July 17 was related to the decomposition and respiration of decaying algae by microorganisms. Previous studies on the *U. prolifera* affecting the carbonate system in the Qingdao coastal area usually focused on the late bloom or after bloom period. These reports also found the release of CO_2 and reduced DO during the late bloom period (Deng et al., 2018; Xiong et al., 2023). However, previous studies were based on limited sample collection, and the effect of *U. prolifera* on carbonate system mostly examined vis incubation experiment, lacking *in-situ* continuous observations (Deng et al., 2018; Xiong et al., 2023). The time series observation in this work captured the significant effect of the continuous changing *U. prolifera* on seawater pCO_2, especially the influence on obvious decrease of seawater pCO_2 at early bloom stage, which confirms that the high-resolution measurements are essential for the study of carbonate system during algal blooms and provides a reference for the future study of the *U. prolifera blooms* influence on carbonate system.

4 Conclusion

The buoy-based time series monitoring seawater pCO_2 near Xiaomaidao Island during summer showed the necessity for high-resolution measurement of pCO_2 in coastal seawater. During the observation period, the surface seawater pCO_2 showed a generally increased trend, with an average value of 615 ± 45 µatm, and it was mainly affected by the increased temperature except for the decreased pCO_2 during July 12-21. We captured the rapid decline and rise of seawater pCO_2 and $npCO_2$ during this special period which was caused by the *U. prolifera* bloom, and the daily mean seawater pCO_2 and $npCO_2$ decreased by 116 µatm and 147 µatm, respectively, compared with the values before decrease. Jiaozhou Bay was a strong source of atmospheric CO_2 during summer, and the observation site was also acted as a CO_2 source. The CO_2 flux of observation site was greatly affected by wind speed and seawater pCO_2, releasing 334 mmol CO_2 m^{-2} throughout the investigation period.

Data availability statement

The raw data supporting the conclusions of this article will be made available by the authors, without undue reservation.

Author contributions

LC: Conceptualization, Data curation, Funding acquisition, Writing – original draft. SL: Formal analysis, Writing – review & editing. SZ: Investigation, Methodology, Writing – review & editing. NWu: Investigation, Writing – review & editing. KZ: Data curation, Writing – review & editing. WL: Investigation, Writing – review & editing. RM: Investigation, Writing – review & editing. DC: Methodology, Writing – review & editing. NWa: Supervision, Writing – review & editing. YL: Supervision, Methodology, Writing – review & editing.

Funding

Conflict of interest

The authors declare that the research was conducted in the absence of any commercial or financial relationships that could be construed as a potential conflict of interest.

Publisher's note

References

Agade, P., Bean, E. Z., Dean, R. N., Blersch, D., Vasconcelos, J., Knappenberger, T., et al. (2022). GatorByte: A Water-Quality Mapping Buoy for Locating Watershed Pollution Sources. *Proceedings of IEEE Sensors*, 2022-October. doi: 10.1109/SENSORS52175.2022.9967172

Alliance for Coastal Technologies (ACT) (2010a). Performance demonstration statement for Contros HydroC^{TM}/CO$_2$, ACT DS10-01 UMCES/CBL 10-091.

Alliance for Coastal Technologies (ACT) (2010b). Performance demonstration statement for Pro-Oceanus Systems Inc. PSI CO$_2$-Pro^{TM}, ACT DS10-03 UMCES/CBL 10-093.

Alliance for Coastal Technologies (ACT) (2010c). Performance demonstration statement for PMEL MAPCO$_2$/Battelle seaology pCO$_2$ monitoring system, ACT DS10-02 UMCES/CBL 10-092.

Atamanchuk, D., Tengberg, A., Aleynik, D., Fietzek, P., Shitashima, K., Lichtschlag, A., et al. (2015). Detection of CO$_2$ leakage from a simulated sub-seabed storage site using three different types of pCO$_2$ sensors. *Int. J. Greenh. Gas Con.* 38, 121–134. doi: 10.1016/j.ijggc.2014.10.021

Błażejewski, A., Pecolt, S., Grunt, M., Wieczorek, G., and Królikowski, T. (2024). Multi-domain, Autonomous measurement buoy as an element of the water quality monitoring and early warning system in rivers and water reservoirs. *Rocznik Ochrona Środowiska* 26, 18–29. doi: 10.54740/ros.2024.002

Błażejewski, A., Pecolt, S., Królikowski, T., Grunt, M., and Bielicki, F. (2023). Project of innovative open multi-domain early warning platform enviwise for adverse events in water bodies and streams. *Proc. Comput. Sci.* 225, 27433–2753. doi: 10.1016/j.procs.2023.10.266

Borges, A. V., Schiettecatte, L. S., Abril, G., Delille, B., and Gazeau, F. (2006). Carbon dioxide in European coastal waters. *Estuar. Coast. Shelf Sci.* 70, 375–387. doi: 10.1016/j.ecss.2006.05.046

Cai, W. J. (2011). Estuarine and coastal ocean carbon paradox: CO2 sinks or sites of terrestrial carbon incineration? *Annu. Rev. Mar. Sci.* 3, 123–145. doi: 10.1146/annurev-marine-120709-142723

Dai, M., Su, J., Zhao, Y., Hofmann, E. E., Cao, Z., Cai, W.-J., et al. (2022). Carbon fluxes in the coastal ocean: synthesis, boundary processes and future trends. *Annu. Rev. Earth PI. SC.* 50, 593–626. doi: 10.1146/annurev-earth-032320-090746

Deng, X., Liu, T., Liu, C. Y., Liang, S. K., Hu, Y. B., Jin, Y. M., et al. (2018). Effects of *Ulva prolifera* blooms on the carbonate system in the coastal waters of Qingdao. *Mar. Ecol. Prog. Ser.* 605, 73–86. doi: 10.3354/meps12739

Doney, S. C., Fabry, V. J., Feely, R. A., and Kleypas, J. A. (2009). Ocean acidification: the other CO$_2$ problem. *Annu. Rev. Mar. Sci.* 1, 169–192. doi: 10.1146/annurev.marine.010908.163834

Fietzek, P., Fiedler, B., Steinhoff, T., and Körtzinger, A. (2014). *In situ* quality assessment of a novel underwater pCO$_2$ sensor based on membrane equilibration and NDIR spectrometry. *J. Atmos. Ocean. Tech.* 31, 181–196. doi: 10.1175/JTECH-D-13-00083.1

Friederich, G. E., Brewer, P. G., Herlien, R., and Chavez, F. P. (1995). Measurement of sea surface partial pressure of CO$_2$ from a moored buoy. *Deep-Sea Res. Pt. I* 42, 1175–1186. doi: 10.1016/0967-0637(95)00044-7

Gao, Z., Yang, D., Qin, J., Xiang, L., and Zhang, K. (2008). The land-sourced pollution in the Jiaozhou Bay. *Chin. J. Oceanol. Limn.* 26, 229–232. doi: 10.1007/s00343-008-0229-7

Hu, Z. X., Li, T., Ge, T. T., Hu, J. W., Wang, P., Liu, C. Y., et al. (2024). Inter-annual and spatial variations of air-sea CO2 fluxes and acidification mechanism in the coastal waters of Qingdao, China during 2011-2019. *Mar. pollut. Bull.* 209, 117195. doi: 10.1016/j.marpolbul.2024.117195

Hu, Y. B., Liu, C. Y., Yang, G. P., and Zhang, H. H. (2015). The response of the carbonate system to a green algal bloom during the post-bloom period in the southern Yellow Sea. *Cont. Shelf Res.* 94, 1–7. doi: 10.1016/j.csr.2014.12.006

Hunt, C. W., Snyder, L., Salisbury, J. E., Vandemark, D., and McDowell, W. H. (2017). SIPCO2: A simple, inexpensive surface water pCO$_2$ sensor. *Limnol. Oceanogr.: Methods* 15, 291–301. doi: 10.1002/lom3.10157

Li, B. H., Liu, C. Y., Deng, X., Wang, K. K., Han, L., Huang, Y. H., et al. (2021). Responses of the marine carbonate system to agreen tide: a case study of an *Ulva prolifera* bloom in Qingdao coastal waters. *Harmful Algae* 110, 102133. doi: 10.1016/j.hal.2021.102133

Li, Y. X., Xue, L., Yang, X. F., Wei, Q. S., Xin, M., Xue, M., et al. (2023). Wastewater inputs reduce the CO$_2$ uptake by coastal oceans. *Sci. Total Environ.* 901, 165700. doi: 10.1016/j.scitotenv.2023.165700

Li, S. X., Yu, K. F., Huo, Y. Z., Zhang, J. H., Wu, H. L., Wu, Q., et al. (2014). The photosynthetic physiological characteristics and evaluation of carbon fixation capacity of *Ulva prolifera* in Binhai sea area, Jiangsu Province. *Mar. Fish* 36, 306–313. doi: 10.13233/j.cnki.mar.fish.2014.04.005

Lin, G., and Lin, X. (2022). Bait input altered microbial community structure and increased greenhouse gases production in coastal wetland sedimen. *Water Res.* 218, 118520. doi: 10.1016/j.watres.2022.118520

Liu, Q., Dong, X., Chen, J. S., Guo, X. H., Zhang, Z. R., Xu, Y., et al. (2019). Diurnal to interannual variability of sea surface pCO$_2$ and its controls in a turbid tidal-driven nearshore system in the vicinity of the East China Sea based on buoy observations. *Mar. Chem.* 216, 103690. doi: 10.1016/j.marchem.2019.103690

Liu, X. Y., Yang, X. F., Li, Y. X., Zang, H., and Zhang, L. J. (2019). Variations in dissolved inorganic carbon species in effluents from large-scale municipal wastewater treatment plants (Qingdao, China) and their potential impacts on coastal acidification. *Environ. Sci. pollut. Res.* 26, 15019–15027. doi: 10.1007/s11356-019-04871-2

Mostofa, K. M. G., Liu, C. Q., Zhai, W., Minella, M., Vione, D., Gao, K., et al. (2016). Reviews and syntheses: ocean acidification and its potential impacts on marine ecosystems. *Biogeosciences* 13, 1767–1786. doi: 10.1196/annals.1439.013

Murata, A., Inoue, J., Nishino, S., and Yasunaka, S. (2022). Early Wintertime CO$_2$ uptake in the western Arctic Ocean. *J. Geophys. Res.-Oceans.* 127, e2021JC018037. doi: 10.1029/2021JC018037

Ng, C. L., Senft-Grupp, S., and Hemond, H. F. (2012). A multi-platform optical sensor for *in situ* sensing of water chemistry. *Limnol. Oceanogr: Methods* 10, 978–990. doi: 10.4319/lom.2012.10.978

Regnier, P., Resplandy, L., Najjar, R. G., and Ciais, P. (2022). The land-to-ocean loops of the global carbon cycle. *Nature* 603, 401–410. doi: 10.1038/s41586-021-04339-9

Ribas-Ribas, M., Kilcher, L. F., and Wurl, O. (2018). Sniffle: A step forward to measure in *situ* CO$_2$ fluxes with the floating chamber technique. *Elem. Sci. Anth.* 6. doi: 10.1525/elementa.275

Sabine, C. L., Feely, R. A., Gruber, N., Key, R. M., Lee, K., and Bullister, J. L. (2004). The oceanic sink for anthropogenic CO$_2$. *Science* 305, 367–371. doi: 10.1126/science.1097403

Shao, K. S., Gong, N., Shen, L. Y., Han, X., Wang, Z. X., Zhou, K., et al. (2024). Why did the world's largest green tides occur exclusively in the southern Yellow Sea? *Mar. Environ. Res.* 200, 106671. doi: 10.1016/j.marenvres.2024.106671

Sutton, A. J., Sabine, C. L., Maenner-Jones, S., Lawrence-Slavas, N., Meinig, C., Feely, R. A., et al. (2014). A high-frequency atmospheric and seawater pCO$_2$ data set from 14 open-ocean sites using a moored autonomous system. *Earth. Syst. Sci. Data.* 6, 353–366. doi: 10.5194/essd-6-353-2014

Sweeney, C., Gloor, E., Jacobson, A. R., Key, R. M., Mckinley, G., Sarmiento, J. L., et al. (2007). Constraining global air-sea gas exchange for CO$_2$ with recent bomb ^{14}C measurements. *Global Biogeochem. Cy* 21, GB2015. doi: 10.1029/2006GB002784

Takahashi, T., Olafsson, J., Goddard, J. G., Chipman, D. W., and Sutherland, S. C. (1993). Seasonal variation of CO$_2$ and nutrients in the high-latitude surface oceans: a comparative study. *Global Biogeochem. Cy.* 7, 843–878. doi: 10.1029/93GB02263

Wang, S. Y., and Zhai, W. D. (2021). Regional differences in seasonal variation of air-sea CO$_2$ exchange in the Yellow Sea. *Cont. Shelf Res.* 218, 104393. doi: 10.1016/j.csr.2021.104393

Wanninkhof, R. (1992). Relationship between wind speed and gas exchange over the Ocean. *J. Geophys. Res.* 97, 7373–7382. doi: 10.1029/92JC00188

Weiss, R. F. (1974). Carbon dioxide in water and seawater: the solubility of a non-ideal gas. *Mar. Chem.* 2, 203–215. doi: 10.1016/0304-4203(74)90015-2

Weiss, R. F., and Price, B. A. (1980). Nitrous oxide solubility in water and seawater. *Mar. Chem.* 8, 347–359. doi: 10.1016/0304-4203(80)90024-9

Wu, Z. L., Wang, H. J., Liao, E. H., Hu, C. M., Edwing, K., Yan, X.-H., et al. (2024). Air-sea CO$_2$ flux in the Gulf of Mexico from observations and multiple machine-learning data products. *Prog. Oceanogr.* 223, 103244. doi: 10.1016/j.pocean.2024.103244

Xiong, T. Q., Li, H. M., Yue, Y. F., Hu, Y. B., Zhai, W. D., Xue, L., et al. (2023). Legacy effects of late macroalgal blooms on dissolved inorganic carbon pool through alkalinity enhancement in coastal ocean. *Environ. Sci. Technol.* 57, 2186–2196. doi: 10.1021/acs.est.2c09261

Xue, L., Cai, W.-J., Hu, X., Sabine, C., Jones, S., Sutton, A. J., et al. (2016). Sea surface carbon dioxide at the Georgia time series site, (2006–2007): Air–sea flux and controlling processes. *Prog. Oceanogr.* 140, 14–26. doi: 10.1016/j.pocean.2015.09.008

Yang, X., Xue, L., Li, Y., Han, P., Liu, X., Zhang, L., et al. (2018). Treated wastewater changes the export of dissolved inorganic carbon and its isotopic composition and leads to acidification in coastal oceans. *Environ. Sci. Technol.* 52, 5590–5599. doi: 10.1021/acs.est.8b00273

Yuan, C., Xiao, J., Zhang, X. L., Zhou, J., and Wang, Z. L. (2022). A new assessment of the algal biomass of green tide in the Yellow Sea. *Mar. pollut. Bull.* 174, 113253. doi: 10.1016/j.marpolbul.2021.113253

Zhang, Y., He, P. M., Li, H. M., Li, G., Liu, J. H., Jiao, F. L., et al. (2019). *Ulva prolifera* green-tide outbreaks and their environmental impact in the Yellow Sea, China. *Natl. Sci. Rev.* 6, 825–838. doi: 10.1093/nsr/nwz026